Article

Hybrid Nanofluid Flow Past a Permeable Moving Thin Needle

Iskandar Waini [1,2], Anuar Ishak [2,]* and Ioan Pop [3]

[1] Fakulti Teknologi Kejuruteraan Mekanikal dan Pembuatan, Universiti Teknikal Malaysia Melaka, Hang Tuah Jaya, Durian Tunggal 76100, Melaka, Malaysia; iskandarwaini@utem.edu.my

[2] Department of Mathematical Sciences, Faculty of Science and Technology, Universiti Kebangsaan Malaysia, UKM Bangi 43600, Selangor, Malaysia

[3] Department of Mathematics, Babeș-Bolyai University, 400084 Cluj-Napoca, Romania; ipop@math.ubbcluj.ro

* Correspondence: anuar_mi@ukm.edu.my

check for updates

Abstract: The problem of a steady flow and heat transfer past a permeable moving thin needle in a hybrid nanofluid is examined in this study. Here, we consider copper (Cu) and alumina (Al$_2$O$_3$) as hybrid nanoparticles, and water as a base fluid. In addition, the effects of thermophoresis and Brownian motion are taken into consideration. A similarity transformation is used to obtain similarity equations, which are then solved numerically using the boundary value problem solver, bvp4c available in Matlab software (Matlab_R2014b, MathWorks, Singapore). It is shown that heat transfer rate is higher in the presence of hybrid nanoparticles. It is discovered that the non-uniqueness of the solutions is observed for a certain range of the moving parameter λ. We also observed that the bifurcation of the solutions occurs in the region of $\lambda < 0$, i.e., when the needle moved toward the origin. Furthermore, we found that the skin friction coefficient and the heat transfer rate at the surface are higher for smaller needle sizes. A reduction in the temperature and nanoparticle concentration was observed with the increasing of the thermophoresis parameter. It was also found that the increase of the Brownian motion parameter leads to an increase in the nanoparticle concentration. Temporal stability analysis shows that only one of the solutions was stable and physically reliable as time evolved.

Keywords: Brownian motion; dual solutions; hybrid nanofluid; stability analysis; thermophoresis; thin needle

1. Introduction

The development of advanced heat transfer fluids has received considerable coverage from the researchers and scientists over the last few years. Regular fluids (ethylene glycol, oil, water) are commonly used in the industrial and engineering applications. However, the heat transfer rate of these fluids is limited due to weak thermal conductivity. Therefore, to resolve its deficiency, a single form of nanosized particles is applied to the above-mentioned fluids and is called 'nanofluid'. This term was introduced by Choi and Eastman [1] for the first time in 1995. To name a few, the advantages of utilizing nanofluids filled in a rectangular enclosure have been examined by Khanafer et al. [2] and Oztop and Abu-Nada [3].

Nevertheless, 'hybrid nanofluid' was developed to upgrade a regular nanofluid's thermal properties. It seems that Turcu et al. [4] and Jana et al. [5] are among the earliest researchers who considered the hybrid nanocomposite particles in their experimental studies. Hybrid nanofluid is an advanced fluid that incorporates more than one nanoparticle which has the capacity of raising the heat transfer rate because of the synergistic effects [6]. In addition, the desired heat transfer can be accomplished by combining or hybridizing the suitable nanoparticles [7].

Over the past few years, the boundary layer flow past a stretched or shrunk surface in a hybrid nanofluid has been extensively investigated. The research in this area was rapidly established due to its important applications in the industrial processes, for example, in paper production, extraction of polymer, artificial fiber and glass blowing. The investigations of the hybrid nanofluid flow over a stretched surface considering 2D and 3D flows were done by Devi and Devi [8,9]. In these studies, they discovered that the larger nanoparticle volume fractions contributed to the enhancement of the heat transfer rate. Furthermore, a new hybrid nanofluid's thermophysical model was introduced in their studies. The validity of this new thermophysical model was achieved by comparing the results with the experimental data from Suresh et al. [10]. Moreover, Hayat and Nadeem [11] studied the problem of a hybrid nanofluid composed of Ag–CuO/water for the three-dimensional rotating flow. In addition, the dual nature of the flow past a stretched and shrunk surface in a hybrid nanofluid with temporal stability analysis was reported by Waini et al. [12]. They discovered that one of the solutions is unstable in the long run, while the other is stable and thus physically reliable. After that, various flows and heat transfer of a hybrid nanofluid were extended to the different aspects by Waini et al. [13–20].

The flow over a thin needle has become a topic of interest for the researchers because of its importance in industrial applications such as the hot wire anemometer, electronic devices and geothermal power generation. The thin needle is viewed as a body of revolution where its thickness is smaller compared to the boundary layer thickness. Historically, Lee [21] initially studied the viscous fluid flow past a thin needle. Then, this work was explored by the researchers [22–29] by considering various physical aspects. Furthermore, in the work of Ishak et al. [30], the dual solutions were obtained when the movement of the needle is in the opposite direction to the free stream. Then, a similar problem was studied by Waini et al. [31] but with the heat flux surface temperature. Apart from that, the effect of the nanoparticle on the flow over a thin needle was initiated by Grosan and Pop [32] and then extended by Soid et al. [33] to a moving needle in a nanofluid. Furthermore, the effect of the magnetic field on the flow past a moving vertical thin needle in a nanofluid was reported by Salleh et al. [34].

This study aims to examine the flow past a permeable moving thin needle in a hybrid nanofluid by employing Tiwari and Das [35] and Buongiorno [36] nanofluid models. Here, we consider water as the base fluid, while copper (Cu) and alumina (Al_2O_3) as the hybrid nanoparticles. Further, the effect of thermophoresis and Brownian motion are also considered. The results are obtained for several physical parameters and presented graphically and through tables. Also, the comparison results for limiting cases are done with previously published data.

2. Mathematical Formulation

The flow configuration past a permeable moving thin needle in a hybrid nanofluid is demonstrated in Figure 1. Here, x and r are the cylindrical coordinates with x- and r- being the axial and radial coordinates, respectively. The needle moves with a constant speed U_∞ in a moving fluid with the same speed U_∞. Furthermore, the surface temperature T_w and the ambient temperature T_∞ are constant such that $T_w > T_\infty$, whereas C_∞ is the ambient nanoparticle concentration with the normal flux of nanoparticles is zero at the wall. The shape of the nanoparticle is spherical, and its size is uniform, while the agglomeration is disregarded since the hybrid nanofluid is formed as a stable composite. After employing the usual boundary layer approximations, the governing equations of the hybrid nanofluid are given by (see Soid et al. [33]; Kuznetsov and Nield [37]):

$$\frac{\partial}{\partial x}(ru) + \frac{\partial}{\partial r}(rv) = 0 \tag{1}$$

$$u\frac{\partial u}{\partial x} + v\frac{\partial u}{\partial r} = \frac{\mu_{hnf}}{\rho_{hnf}}\frac{1}{r}\frac{\partial}{\partial r}\left(r\frac{\partial u}{\partial r}\right) \tag{2}$$

$$u\frac{\partial T}{\partial x} + v\frac{\partial T}{\partial r} = \frac{1}{r}\frac{k_{hnf}}{(\rho C_p)_{hnf}}\frac{\partial}{\partial r}\left(r\frac{\partial T}{\partial r}\right) + \sigma\left[D_B\frac{\partial C}{\partial r}\frac{\partial T}{\partial r} + \frac{D_T}{T_\infty}\left(\frac{\partial T}{\partial r}\right)^2\right] \tag{3}$$

$$u\frac{\partial C}{\partial x} + v\frac{\partial C}{\partial r} = \frac{D_B}{r}\frac{\partial}{\partial r}\left(r\frac{\partial C}{\partial r}\right) + \frac{D_T}{T_\infty}\frac{1}{r}\frac{\partial}{\partial r}\left(r\frac{\partial T}{\partial r}\right) \tag{4}$$

subject to:

$$u = U_\infty\lambda, \ v = v_w, \ T = T_w, \ D_B\frac{\partial C}{\partial r} + \frac{D_T}{T_\infty}\frac{\partial T}{\partial r} = 0 \text{ at } r = R(x)$$
$$u \to U_\infty, \ T \to T_\infty, \ C \to C_\infty \text{ as } r \to \infty \tag{5}$$

where the surface of the thin needle is described by $R(x)$, u and v are the velocity components in the axial x- and radial r- directions, D_T and D_B are thermophoretic diffusion and Brownian diffusion coefficients, respectively. Additionally, σ, T, C and v_w represent the effective heat capacity ratio, hybrid nanofluid's temperature, nanoparticle concentration and mass flux velocity.
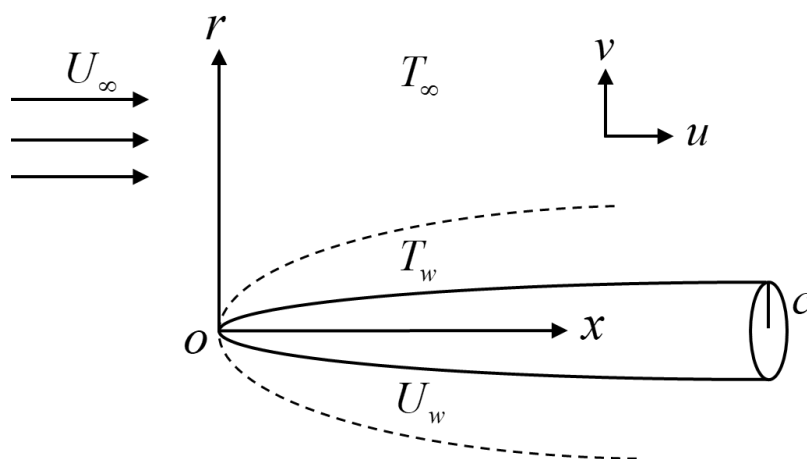

Figure 1. Physical model.

Further, $\left(\rho C_p\right)_{hnf}$, k_{hnf}, μ_{hnf}, and ρ_{hnf} characterize the heat capacity, thermal conductivity, dynamic viscosity and density of the hybrid nanofluid, respectively, where their thermophysical properties are defined in Table 1. Meanwhile, the physical properties of Cu, Al$_2$O$_3$ and water are given in Table 2. Here, k, ρ, μ, $\left(\rho C_p\right)$, and C_p represent the thermal conductivity, density, dynamic viscosity, heat capacity and specific heat at constant pressure, respectively. Meanwhile, the nanoparticle volume fractions of Al$_2$O$_3$ and Cu are symbolized by φ_1 and φ_2, while their solid components are indicated by the subscripts $n1$ and $n2$, respectively. In addition, the hybrid nanofluid, nanofluid and fluid, are indicated by the subscripts hnf, nf and f, respectively.

Table 1. Thermophysical properties of nanofluid and hybrid nanofluid (see [3,8,15]).

Thermophysical Properties	Nanofluid	Hybrid Nanofluid
Density	$\rho_{nf} = (1-\varphi_1)\rho_f + \varphi_1\rho_{n1}$	$\rho_{hnf} = (1-\varphi_2)\left[(1-\varphi_1)\rho_f + \varphi_1\rho_{n1}\right] + \varphi_2\rho_{n2}$
Heat capacity	$(\rho C_p)_{nf} = (1-\varphi_1)(\rho C_p)_f + \varphi_1(\rho C_p)_{n1}$	$(\rho C_p)_{hnf} = (1-\varphi_2)\left[(1-\varphi_1)(\rho C_p)_f + \varphi_1(\rho C_p)_{n1}\right] + \varphi_2(\rho C_p)_{n2}$
Dynamic viscosity	$\mu_{nf} = \dfrac{\mu_f}{(1-\varphi_1)^{2.5}}$	$\mu_{hnf} = \dfrac{\mu_f}{(1-\varphi_1)^{2.5}(1-\varphi_2)^{2.5}}$
Thermal conductivity	$\dfrac{k_{nf}}{k_f} = \dfrac{k_{n1}+2k_f-2\varphi_1(k_f-k_{n1})}{k_{n1}+2k_f+\varphi_1(k_f-k_{n1})}$	$\dfrac{k_{hnf}}{k_{nf}} = \dfrac{k_{n2}+2k_{nf}-2\varphi_2(k_{nf}-k_{n2})}{k_{n2}+2k_{nf}+\varphi_2(k_{nf}-k_{n2})}$ where $\dfrac{k_{nf}}{k_f} = \dfrac{k_{n1}+2k_f-2\varphi_1(k_f-k_{n1})}{k_{n1}+2k_f+\varphi_1(k_f-k_{n1})}$

Table 2. Thermophysical properties of nanoparticles and water (see [3,15]).

Thermophysical Properties	Al$_2$O$_3$	Cu	Water
$\rho\ (kg/m^3)$	3970	8933	997.1
$C_p\ (J/kgK)$	765	385	4179
$k\ (W/mK)$	40	400	0.613
Prandtl number, Pr			6.2

An appropriate transformation is introduced as follows (see Soid et al. [33] and Kuznetsov and Nield [37]):

$$\psi = v_f x\, f(\eta), \ \theta(\eta) = \frac{T - T_\infty}{T_w - T_\infty}, \ \phi(\eta) = \frac{C - C_\infty}{C_\infty}, \ \eta = \frac{U_\infty\, r^2}{v_f\, x} \tag{6}$$

where ψ denotes the stream function with $u = (1/r)(\partial\psi/\partial r)$ and $v = -(1/r)(\partial\psi/\partial x)$ so that Equation (1) is identically satisfied. Thus, we have:

$$u = 2U_\infty f'(\eta), \ v = -\frac{v_f}{r}(f(\eta) - \eta f'(\eta)) \tag{7}$$

and,

$$v_w = -\frac{v_f}{r}\frac{\lambda}{2}c \tag{8}$$

where primes denote differentiation with respect to η and v_f is the fluid's kinematic viscosity. Setting $\eta = c$ (refer to the wall of the needle) in Equation (6), the needle's surface can be defined as:

$$R(x) = \left(\frac{v_f c\, x}{U_\infty}\right)^{1/2} \tag{9}$$

Using (6), Equations (2) to (4) become:

$$2\frac{\mu_{hnf}/\mu_f}{\rho_{hnf}/\rho_f}(\eta f'')' + f f'' = 0 \tag{10}$$

$$\frac{2}{\mathrm{Pr}}\frac{k_{hnf}/k_f}{(\rho C_p)_{hnf}/(\rho C_p)_f}(\eta\theta')' + f\theta' + 2\eta\left(Nb\phi'\theta' + Nt\theta'^2\right) = 0 \tag{11}$$

$$2(\eta\phi')' + Scf\phi' + 2\frac{Nt}{Nb}(\eta\theta')' = 0 \tag{12}$$

subject to:

$$f(c) = \lambda c, \ f'(c) = \tfrac{\lambda}{2}, \ \theta(c) = 1, \ Nb\phi'(c) + Nt\theta'(c) = 0$$
$$f'(\eta) \to \tfrac{1}{2}, \ \theta(\eta) \to 0, \ \phi(\eta) \to 0 \text{ as } \eta \to \infty \tag{13}$$

Here, Pr represents the Prandtl number, Sc is the Schmidt number, Nt and Nb denote the thermophoresis and Brownian motion parameters, respectively and λ is the constant moving parameter. The needle moves away from the origin if $\lambda > 0$ and moves toward the origin if $\lambda < 0$. All these parameters are defined as:

$$\mathrm{Pr} = \frac{(\mu C_p)_f}{k_f}, \ Sc = \frac{v_f}{D_B}, \ Nt = \frac{\sigma\, D_T\,(T_w - T_\infty)}{v_f\, T_\infty}, \ Nb = \frac{\sigma\, D_B\, C_\infty}{v_f} \tag{14}$$

The physical quantities of interest are the skin friction coefficient C_f, the local Nusselt number Nu_x and the local Sherwood number Sh_x which are defined as

$$C_f = \frac{\tau_w}{\rho_f\, U_\infty^2}, \ Nu_x = \frac{x\, q_w}{k_f\,(T_w - T_\infty)}, \ Sh_x = \frac{x\, q_m}{D_B\, C_\infty}, \tag{15}$$

where the shear stress along the surface of the needle τ_w, the heat flux q_w and the mass flux from the surface of the needle q_m are given by

$$\tau_w = \mu_{hnf}\left(\frac{\partial u}{\partial r}\right)_{r=R(x)}, \ q_w = -k_{hnf}\left(\frac{\partial T}{\partial r}\right)_{r=R(x)}, \ q_m = -D_B\left(\frac{\partial C}{\partial r}\right)_{r=R(x)} \tag{16}$$

Using (6), (15) and (16), we get

$$
\begin{aligned}
Re_x^{1/2}C_f &= 4c^{1/2}\frac{\mu_{hnf}}{\mu_f}f''(0), \ Re_x^{-1/2}Nu_x = -2c^{\frac{1}{2}}\frac{k_{hnf}}{k_f}\theta'(c) \\
Re_x^{-1/2}Sh_x &= -2c^{1/2}\phi'(c) = 2c^{1/2}\frac{Nt}{Nb}\theta\prime(c),
\end{aligned}
\tag{17}
$$

where $Re_x = U_\infty x/\nu_f$ is the local Reynolds number. Note that, the reduced Sherwood number follows the reduced Nusselt number due to the passive control condition in Equation (13) for $Nb = Nt$. The effect of the changes in the boundary condition is instantly obvious where the parameters Nb and Nt now appear in the boundary conditions as well as in the differential equations.

3. Stability Analysis

The existence of the non-uniqueness solutions of Equations (10) to (13) is observed for a certain range of the physical parameters. A temporal stability analysis is therefore needed to determine which solution is stable and thus physically reliable in the long run. This technique was initiated by Merkin [38] in 1986. A dimensionless time variable τ was introduced by Weidman et al. [39] to further study the stability of the solutions as time passes. They concluded that the first solutions are stable, while the second solutions are unstable. As in Weidman et al. [39], the new variables based on Equation (6) are given as

$$
\psi = \nu_f x f(\eta, \tau), \ \theta(\eta, \tau) = \frac{T - T_\infty}{T_w - T_\infty}, \ \phi(\eta, \tau) = \frac{C - C_\infty}{C_\infty}, \ \eta = \frac{U_\infty r^2}{\nu_f x}, \ \tau = \frac{2U_\infty t}{x}
\tag{18}
$$

The unsteady form of Equations (1) to (4) are considered to analyze the stability of the solutions. Using (18) and following the similar approach as in Section 2, we get

$$
2\frac{\mu_{hnf}/\mu_f}{\rho_{hnf}/\rho_f}\frac{\partial}{\partial\eta}\left(\eta\frac{\partial^2 f}{\partial\eta^2}\right) + f\frac{\partial^2 f}{\partial\eta^2} - \frac{\partial^2 f}{\partial\eta\,\partial\tau} - \tau\left(\frac{\partial f}{\partial\tau}\frac{\partial^2 f}{\partial\eta^2} - \frac{\partial f}{\partial\eta}\frac{\partial^2 f}{\partial\eta\partial\tau}\right) = 0
\tag{19}
$$

$$
\frac{2}{Pr}\frac{k_{hnf}/k_f}{(\rho C_p)_{hnf}/(\rho C_p)_f}\frac{\partial}{\partial\eta}\left(\eta\frac{\partial\theta}{\partial\eta}\right) + f\frac{\partial\theta}{\partial\eta} + 2\eta\left(Nb\frac{\partial\phi}{\partial\eta}\frac{\partial\theta}{\partial\eta} + Nt\left(\frac{\partial\theta}{\partial\eta}\right)^2\right) - \frac{\partial\theta}{\partial\tau} - \tau\left(\frac{\partial f}{\partial\tau}\frac{\partial\theta}{\partial\eta} - \frac{\partial f}{\partial\eta}\frac{\partial\theta}{\partial\tau}\right) = 0
\tag{20}
$$

$$
2\frac{\partial}{\partial\eta}\left(\eta\frac{\partial\phi}{\partial\eta}\right) + Scf\frac{\partial\phi}{\partial\eta} + 2\frac{Nt}{Nb}\frac{\partial}{\partial\eta}\left(\eta\frac{\partial\theta}{\partial\eta}\right) - Sc\frac{\partial\phi}{\partial\tau} - Sc\tau\left(\frac{\partial f}{\partial\tau}\frac{\partial\phi}{\partial\eta} - \frac{\partial f}{\partial\eta}\frac{\partial\phi}{\partial\tau}\right) = 0
\tag{21}
$$

subject to:

$$
\begin{aligned}
f(c, \tau) - \tau\frac{\partial f}{\partial\tau}(c, \tau) &= \lambda c, \ \frac{\partial f}{\partial\eta}(c, \tau) = \frac{\lambda}{2}, \ \theta(c, \tau) = 1, \ Nb\frac{\partial\phi}{\partial\eta}(c, \tau) + Nt\frac{\partial\theta}{\partial\eta}(c, \tau) = 0 \\
\frac{\partial f}{\partial\eta}(\eta, \tau) &\to \tfrac{1}{2}, \ \theta(\eta, \tau) \to 0, \ \phi(\eta, \tau) \to 0 \text{ as } \eta \to \infty.
\end{aligned}
\tag{22}
$$

To examine the stability behavior, the disturbance is imposed to the steady solution $f(\eta) = f_0(\eta)$, $\theta(\eta) = \theta_0(\eta)$ and $\phi(\eta) = \phi_0(\eta)$ of Equations (10) to (13) by using the following relations (see [39]):

$$
\begin{aligned}
f(\eta, \tau) &= f_0(\eta) + e^{-\gamma\tau}F(\eta), \ \theta(\eta, \tau) = \theta_0(\eta) + e^{-\gamma\tau}G(\eta), \\
\phi(\eta, \tau) &= \phi_0(\eta) + e^{-\gamma\tau}H(\eta),
\end{aligned}
\tag{23}
$$

where γ indicates the unknown eigenvalue that determines the stability of the solutions and $F(\eta)$, $G(\eta)$ and $H(\eta)$ are comparatively small to $f_0(\eta)$, $\theta_0(\eta)$ and $\phi_0(\eta)$. The disturbance is taken exponentially as it demonstrates the rapid decline or development of the disturbance. By inserting Equation (23) into Equations (19) to (21) and by setting $\tau = 0$, we obtain

$$
2\frac{\mu_{hnf}/\mu_f}{\rho_{hnf}/\rho_f}(\eta F'')' + f_0 F'' + f_0'' F + \gamma F' = 0
\tag{24}
$$

$$\frac{2}{\text{Pr}}\frac{k_{hnf}/k_f}{(\rho\,C_p)_{hnf}/(\rho\,C_p)_f}(\eta G')' + f_0 G' + \theta_0' F$$
$$+2\eta\Big(Nb\phi_0'G' + Nb\theta_0'H' + 2Nt\theta_0'G'\Big) + \gamma G = 0 \tag{25}$$

$$2(\eta H')' + Scf_0 H' + Sc\phi_0'F + 2\frac{Nt}{Nb}(\eta G')' + \gamma ScH = 0 \tag{26}$$

subject to:

$$F(c) = 0, \; F'(c) = 0, \; G(c) = 0, \; NbH'(c) + NtG'(c) = 0$$
$$F'(\eta) \to 0, \; G(\eta) \to 0, \; H(\eta) \to 0 \text{ as } \eta \to \infty \tag{27}$$

Without loss of generality, the values of γ from Equations (24) to (27) are obtained for the case of $F''(c) = 1$ as suggested and discussed by Harris et al. [40].

4. Numerical Method

The bvp4c solver in Matlab software (Matlab_R2014b, MathWorks, Singapore) is utilized for evaluating the Equations (10) to (13), numerically. As described in Shampine et al. [41], the aforesaid solver occupies a finite difference method that employs the 3-stage Lobatto IIIa formula. The selection of the initial guess and the boundary layer thickness, η_∞ are particular depend on the parameters applied to obtain the solutions. Moreover, several researchers [42–46] are also employing this solver for solving the boundary layer flow problems. First, Equations (10) to (12) are reduced to a system of ordinary differential equations of the first order. Now, Equation (10) may be written as

$$f = y(1)$$
$$f' = y'(1) = y(2) \tag{28a}$$

$$f'' = y'(2) = y(3) \tag{28b}$$

$$f''' = y'(3) = -\frac{1}{2\eta}\left\{\frac{\rho_{hnf}/\rho_f}{\mu_{hnf}/\mu_f}y(1)y(3) + 2y(3)\right\} \tag{28c}$$

while Equation (11) reduces to:

$$\theta = y(4)$$
$$\theta' = y'(4) = y(5) \tag{29a}$$

$$\theta'' = y'(5) = -\frac{1}{2\eta}\left\{\text{Pr}\frac{(\rho C_p)_{hnf}/(\rho C_p)_f}{k_{hnf}/k_f}\Big[y(1)y(5) + 2\eta\big(Nby(7)y(5) + Nty(5)^2\big)\Big] + 2y(5)\right\} \tag{29b}$$

and Equation (12) reduces to:

$$\phi = y(6)$$
$$\phi' = y'(6) = y(7) \tag{30a}$$

$$\phi'' = y'(7) = -\frac{1}{2\eta}\left\{Scy(1)y(7) + 2\frac{Nt}{Nb}(\eta y(5))' + 2y(7)\right\} \tag{30b}$$

with the boundary conditions:

$$ya(1) = \lambda c, \; ya(2) = \tfrac{\lambda}{2}, \; ya(4) = 1, \; Nbya(7) + Ntya(5) = 0$$
$$yb(2) \to \tfrac{1}{2}, \; yb(4) \to 0, \; yb(6) \to 0 \tag{31}$$

Then, Equations (28) to (31) are coded in Matlab software (Matlab_R2014b, MathWorks, Singapore) and their solutions are obtained by the bvp4c solver. The solver will then run, and the outcomes will be printed out as numerical solutions and graphs.

5. Results and Discussion

In the present study, we consider various volume fractions of Cu (φ_2), while the volume fraction of Al_2O_3 is kept fixed at $\varphi_1 = 0.1$ and water as the base fluid. To ensure the accuracy of the computation, the present results are validated with the existing data from the previous studies. The values of $f''(c)$ and $-\theta'(c)$ when $\varphi_1 = \varphi_2 = 0$ (regular fluid), $\lambda = Sc = 0$ and $Pr = 0.733$ for various values of c in the absence of Nt and Nb are displayed in Tables 3 and 4, respectively. The results are comparable with those obtained by the previous studies. On the other hand, Table 5 is provided to describe the values of $f''(c)$ and $-\theta'(c)$ for Cu/water nanofluid when $\varphi_1 = \lambda = Sc = 0$ and $Pr = 7$ with various values of c and φ_2 in the absence of Nt and Nb. The present numerical results are compared with the previous results obtained by Grosan and Pop [32] and show a favorable agreement. The increment values of $f''(c)$ and $-\theta'(c)$ are observed for the smaller needle size as can be seen in Tables 3–5. It is also observed that the increasing values of φ_2 tend to increase the values of $f''(c)$ but decrease the values of $-\theta'(c)$ as shown in Table 5.

Table 3. Values of $f''(c)$ for regular fluid $(\varphi_1 = \varphi_2 = 0)$ when $\lambda = 0$ with various values of c.

c	Chen and Smith [26]	Ishak et al. [30]	Grosan and Pop [32]	Soid et al. [33]	Present Results
0.1	1.28881	1.2888	1.289074	1.288778	1.288778
0.01	8.49244	8.4924	8.492173	8.491454	8.491454
0.001	62.16372	62.1637	62.161171		62.158227

Table 4. Values of $-\theta'(c)$ for regular fluid $(\varphi_1 = \varphi_2 = 0)$ when $\lambda = Sc = 0$ and $Pr = 0.733$ for various values of c in the absence of Nt and Nb.

c	Chen and Smith [26]	Grosan and Pop [32]	Present Results
0.1	2.434	2.441675	2.439692
0.01		16.306544	16.283107
0.001		120.55034	120.264815

Table 5. Values of $f''(c)$ and $-\theta'(c)$ for Cu/water nanofluid when $\varphi_1 = \lambda = Sc = 0$ and $Pr = 7$ for various values of c and φ_2 in the absence of Nt and Nb.

c	φ_2	$f''(c)$		$-\theta'(c)$	
		Grosan and Pop [32]	Present Results	Grosan and Pop [32]	Present Results
0.1	0.05	1.347208	1.347125	3.682009	3.681817
	0.1	1.382008	1.381635	3.586544	3.586427
	0.2	1.404136	1.404050	3.389762	3.389682
0.01	0.05	8.771680	8.771503	22.284916	22.284751
	0.1	8.935933	8.935143	21.816182	21.816075
	0.2	9.041011	9.040694	20.877668	20.877591
0.001	0.05	63.884384	63.718195	153.570113	153.569704
	0.1	64.653616	64.621235	150.977665	150.977406
	0.2	65.235057	65.200519	145.860889	145.860701

The plots of $f''(c)$ and $-\theta'(c)$ for selected parameters with various values of φ_2 and c against λ are portrayed in Figures 2–5, respectively. Results show that dual solutions exist for a certain range of λ. We observe that the critical values λ_c increase and move slightly to the right with the increasing of φ_2 and c. From our computation, $\lambda_c = -1.13048, -1.10314$ and -1.08436 are the critical values for $\varphi_2 = 0.01, 0.05$ and 0.1, respectively as shown in Figures 2 and 3. Furthermore, the increasing of φ_2 has the tendency to decrease the skin friction coefficient for $\lambda < -0.7$ but increase the heat transfer rate for $\lambda < -0.3$. We also observe that the heat transfer rate is almost the same for $\lambda = -0.3$. Meanwhile, the critical values of λ for $c = 0.1$ and 0.2 are $\lambda_c = -1.08436$ and -0.90271 as can be seen in Figures 4 and 5. It is observed that the values of $f''(c)$ and $-\theta'(c)$ are greater for smaller c.
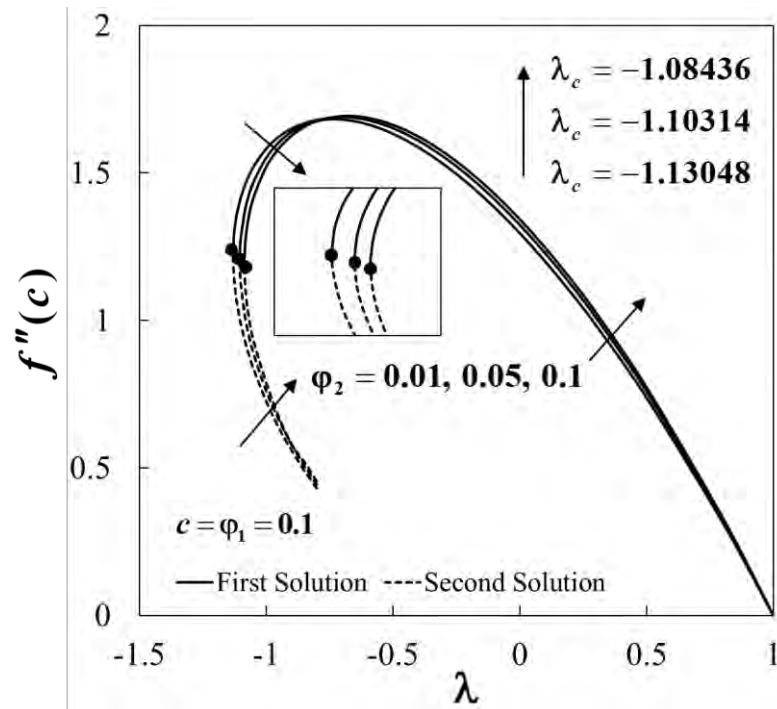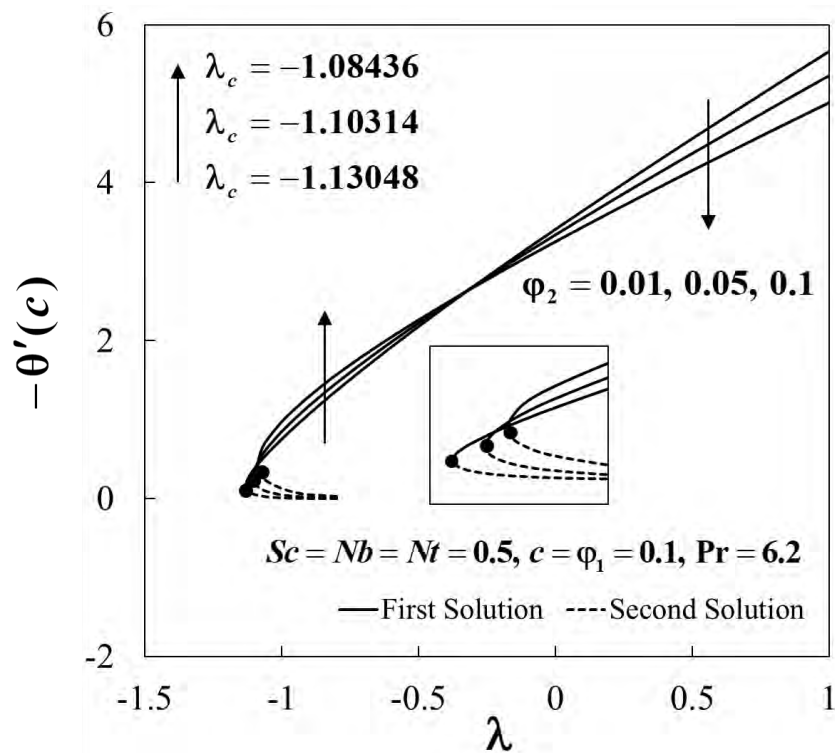
Figure 2. Impact of λ and φ_2 on $f''(c)$.

Figure 3. Impact of λ and φ_2 on $-\theta'(c)$.
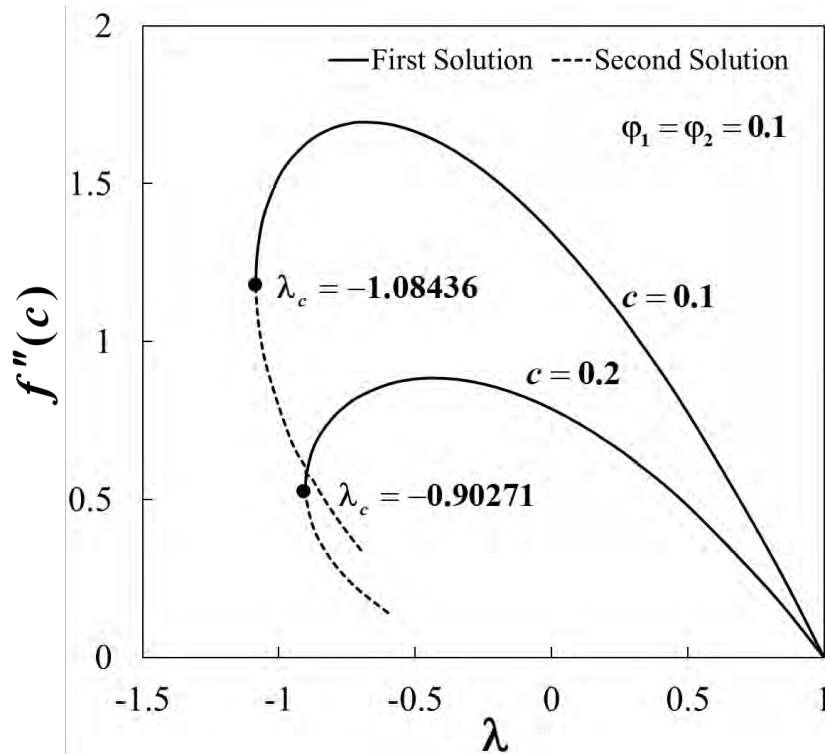
Figure 4. Impact of λ and c on $f''(c)$.
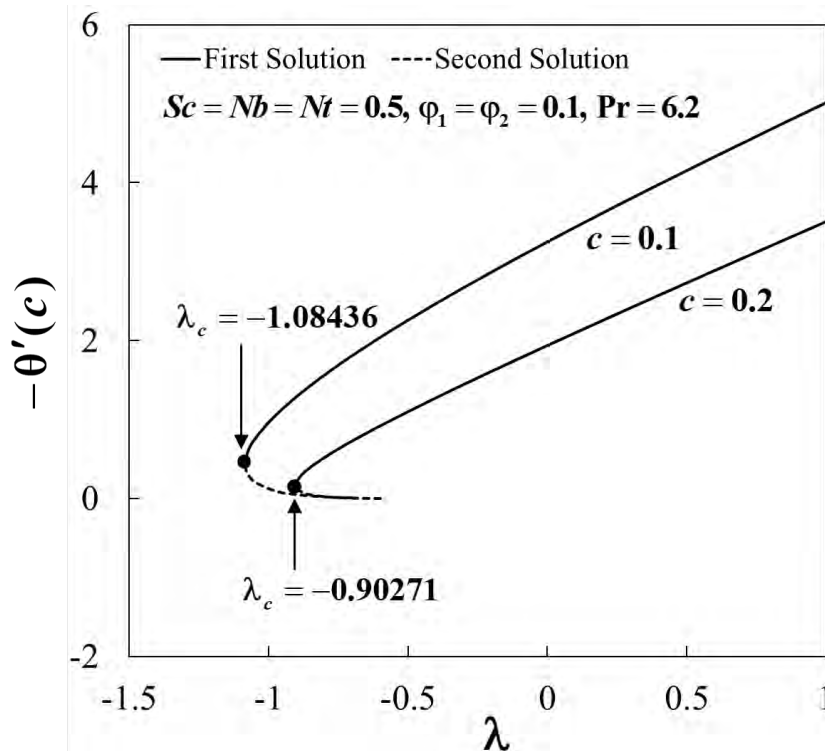

Figure 5. Impact of λ and c on $-\theta'(c)$.

The impact of several parameters on the velocity $f'(\eta)$, temperature $\theta(\eta)$ and nanoparticle concentration $\phi(\eta)$ profiles are presented in Figures 6–14. These profiles asymptotically satisfy the free stream conditions (13), thus giving us confidence in the accuracy of the numerical solutions. Figures 6–8 depict the effect of φ_2 on velocity profiles $f'(\eta)$, temperature profiles $\theta(\eta)$ and concentration profiles $\phi(\eta)$ when $\lambda = -1$, $Sc = Nb = Nt = 0.5$, $c = \varphi_1 = 0.1$ and $Pr = 6.2$. Small effects are observed

for the first solutions (upper branch) of $f'(\eta)$, $\theta(\eta)$ and $\phi(\eta)$ with rising φ_2, but the effects are more pronounced for the second solutions (lower branch).
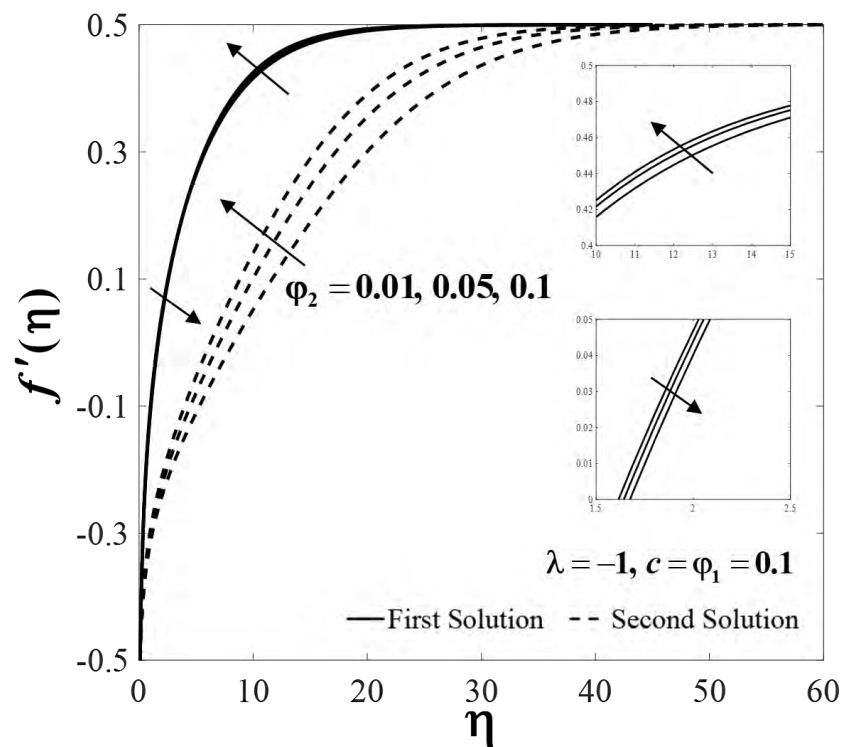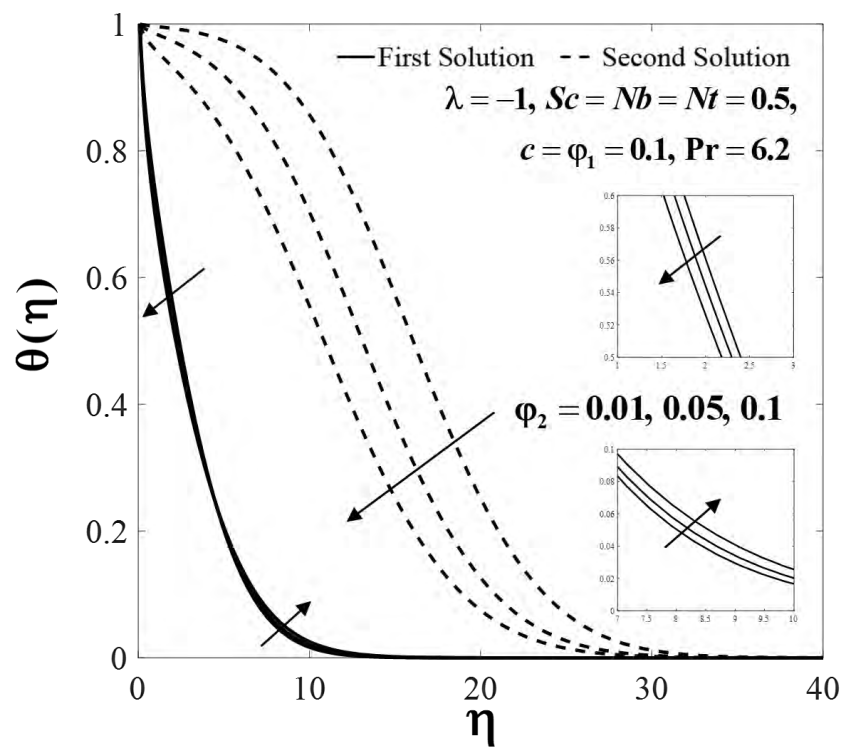

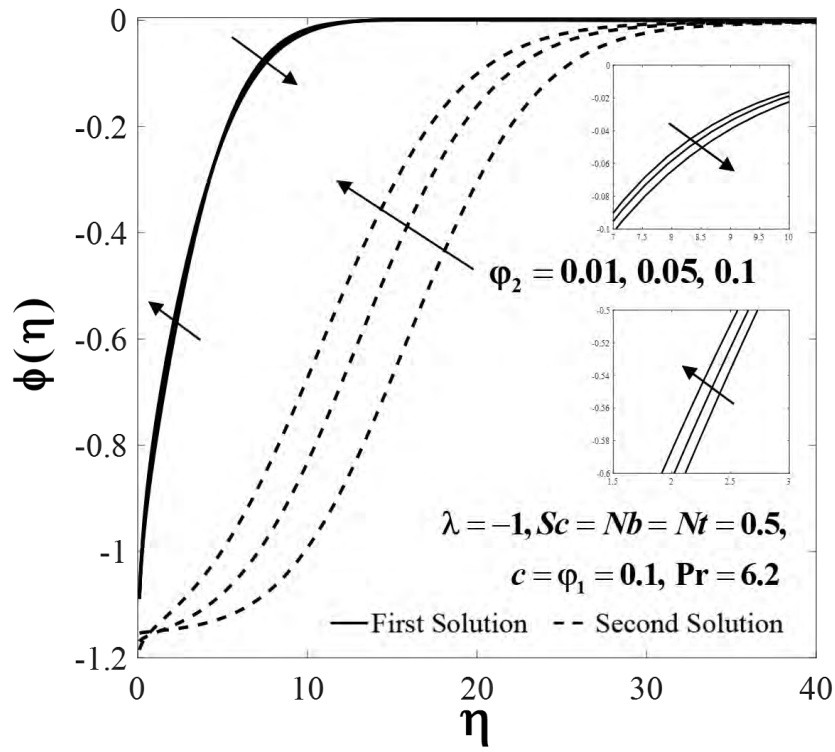**Figure 6.** Impact of φ_2 on $f'(\eta)$.

Figure 7. Impact of φ_2 on $\theta(\eta)$.

Figure 8. Impact of φ_2 on $\phi(\eta)$.
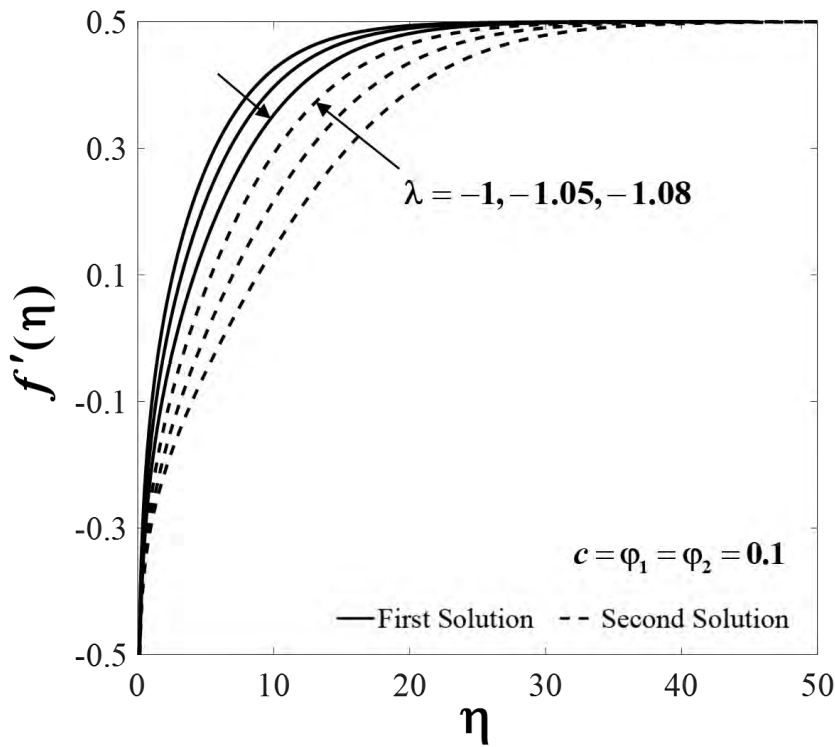
Figure 9. Impact of λ on $f'(\eta)$.
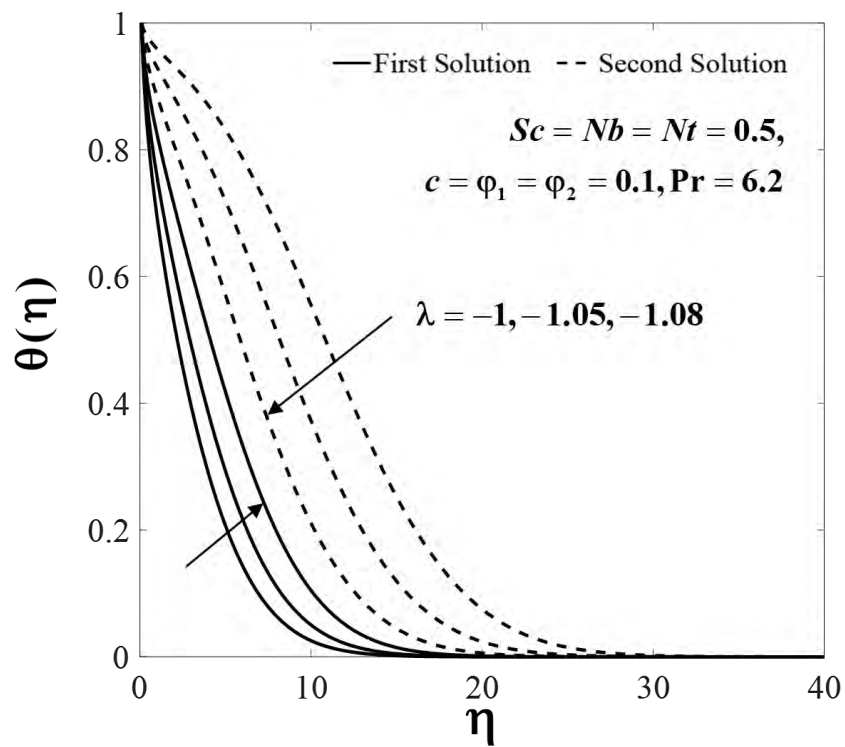
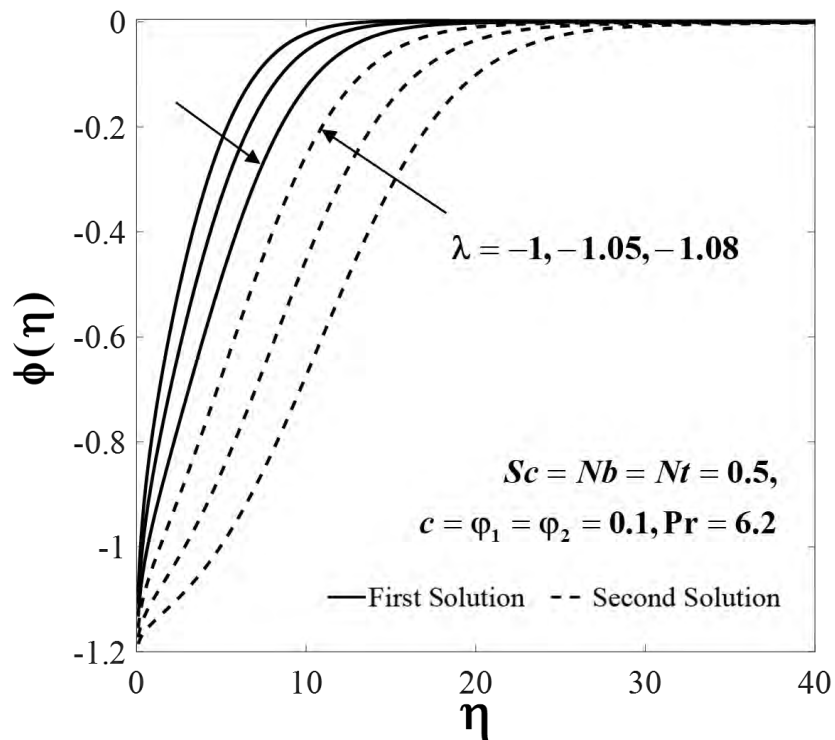**Figure 10.** Impact of λ on $\theta(\eta)$.

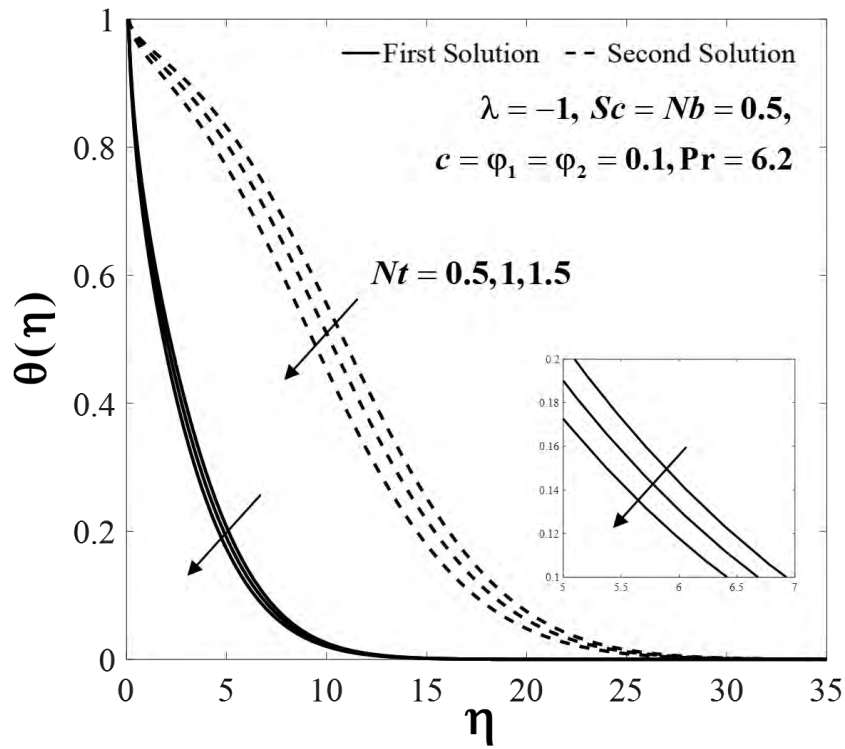**Figure 11.** Impact of λ on $\phi(\eta)$.

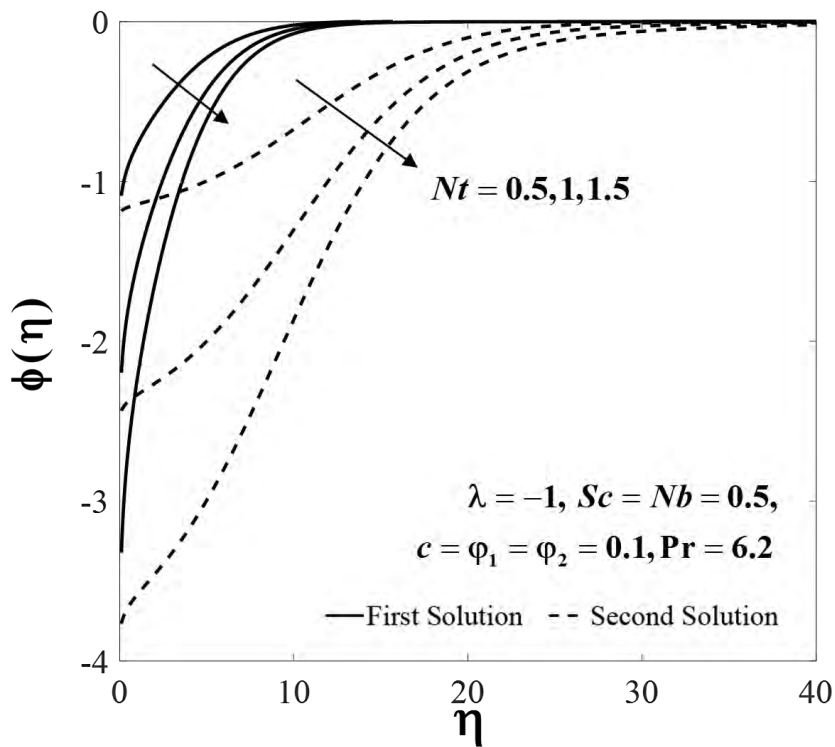**Figure 12.** Impact of Nt on $\theta(\eta)$.

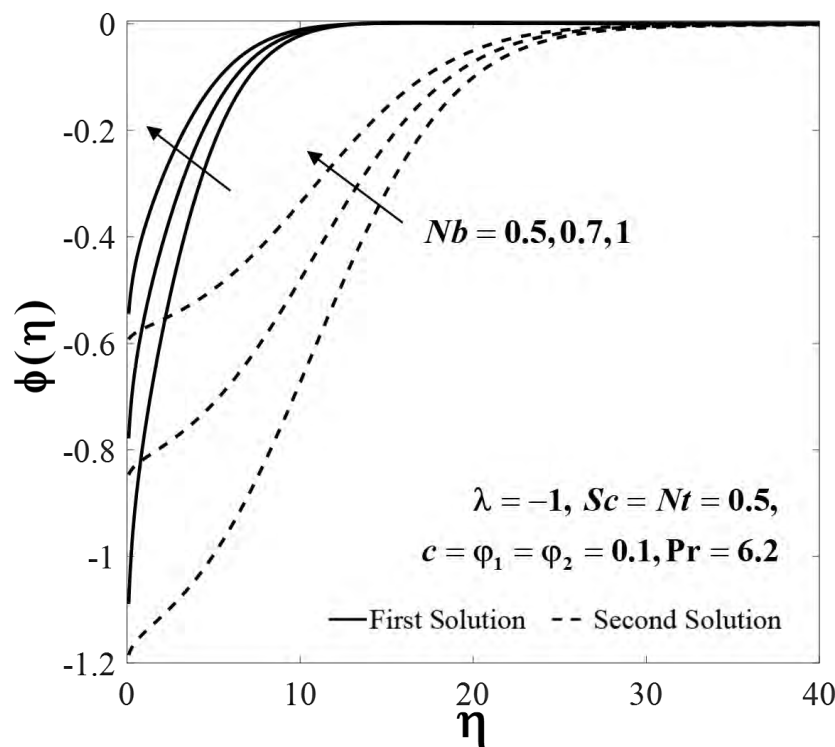**Figure 13.** Impact of Nt on $\phi(\eta)$.

Figure 14. Impact of Nb on $\phi(\eta)$.

The profiles of $f'(\eta)$, $\theta(\eta)$ and $\phi(\eta)$ for different values of λ when $Sc = Nb = Nt = 0.5$, $c = \varphi_1 = \varphi_2 = 0.1$ and $\Pr = 6.2$ are plotted in Figures 9–11, respectively. It is observed that the first solution approaching the second solution as the critical value λ_c is approached. This observation is consistent with the results presented in Figures 2–5. Moreover, the effect of Nt on $\theta(\eta)$ and $\phi(\eta)$ when $\lambda = -1$, $Sc = Nb = 0.5$, $c = \varphi_1 = \varphi_2 = 0.1$ and $\Pr = 6.2$ are displayed in Figures 12 and 13. It is clear that $\theta(\eta)$ and $\phi(\eta)$ decrease for both branches as Nt increases. Figure 14 exhibits the behavior of $\phi(\eta)$ with the variation of Nb when $\lambda = -1$, $Sc = Nt = 0.5$, $c = \varphi_1 = \varphi_2 = 0.1$ and $\Pr = 6.2$. A rise in Nb produces an increase of $\phi(\eta)$ for both branches. Obviously, $\theta(\eta)$ does not affected by Nb due to the passive control condition applied in (13) and consequently, the energy Equation (11) does not contain the parameter Nb.

Figure 15 displays the smallest eigenvalue γ against λ when $c = \varphi_1 = \varphi_2 = 0.1$. As described in Equation (23), the flow is stable when there is an initial decay of disturbance as time passes, i.e., $e^{-\gamma\tau} \to 0$ as $\tau \to \infty$. This will happen for $\gamma > 0$. Meanwhile, the flow is unstable for $\gamma < 0$ due to the initial growth of disturbance as $\tau \to \infty$. From Figure 15, we notice that the values of γ are positive for the first solutions (upper branch), while they are negative for the second solutions (lower branch). Also, the values of γ approach to zero for both branches when $\lambda \to \lambda_c = -1.08436$. Thus, this finding confirms that the first solutions are stable and physically reliable in the long run, while the second solutions are not. Furthermore, we also conclude that the bifurcation of the solutions happens at the critical value $\lambda = \lambda_c$.
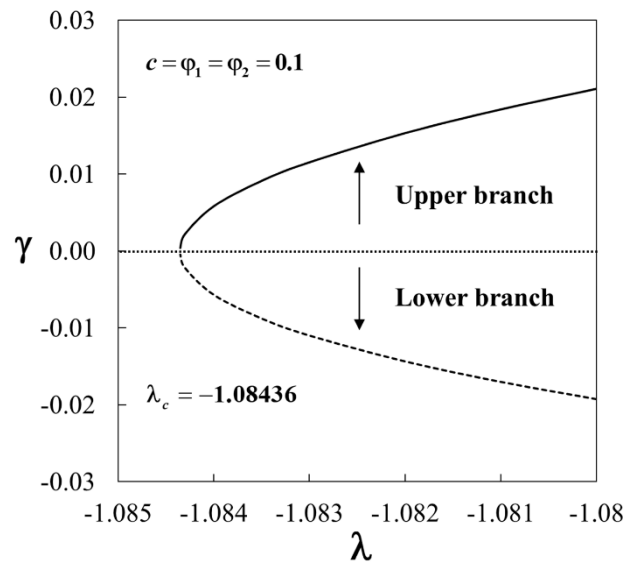
Figure 15. Plot of γ against λ.

6. Conclusions

In this paper, the flow past a permeable moving thin needle in a hybrid nanofluid with thermophoresis and Brownian motion effects was studied. The results validation was done for the limiting cases where the present results are comparable with the existing results. The present results revealed that the added hybrid nanoparticles led to the increment of the heat transfer rate. Dual solutions were obtained for a certain range of the constant moving parameter λ. Furthermore, it was discovered that the bifurcation of the solutions occurs in the region $\lambda < 0$, i.e., when the needle moved toward the origin. The critical values of λ slightly increased for larger values of φ_2 and c. Furthermore, the values of $f''(c)$ and $-\theta'(c)$ are higher for smaller c. It was also observed that $\theta(\eta)$ and $\phi(\eta)$ decreased for larger values of Nt. The increase of Nb led to an increase in $\phi(\eta)$. It was shown that between the two solutions, only one of them is stable, while the other is unstable as time evolved.

Author Contributions: Conceptualization, I.P.; funding acquisition, A.I.; methodology, I.W.; Project administration, A.I.; supervision, A.I. and I.P.; validation, I.P.; writing—original draft, I.W.; writing—review and editing, A.I., I.P. All authors have read and agreed to the published version of the manuscript.

Conflicts of Interest: The authors declare no conflict of interest.

Nomenclature

c	needle size
C	nanoparticle concentration
C_∞	ambient nanoparticle concentration
C_f	skin friction coefficient
C_p	specific heat at constant pressure ($Jkg^{-1}K^{-1}$)
D_B	Brownian diffusion coefficient
D_T	thermophoretic diffusion coefficient
(ρC_p)	heat capacitance of the fluid ($JK^{-1}m^{-3}$)
$f(\eta)$	dimensionless stream function
k	thermal conductivity of the fluid ($Wm^{-1}K^{-1}$)

Nu_x	local Nusselt number
Nb	Brownian motion parameter
Nt	thermophoresis parameter
Pr	Prandtl number
$R(x)$	surface of the needle
Sc	Schmidt number
Sh_x	local Sherwood number
q_m	surface mass flux (Wm^{-2})
q_w	surface heat flux (Wm^{-2})
Re_x	local Reynolds number
T	fluid temperature (K)
T_w	surface temperature (K)
T_∞	ambient temperature (K)
t	time (s)
u, v	velocity components in the x and r directions (ms^{-1})
U_∞	velocity of the needle and the mainstream (ms^{-1})
v_w	velocity of the wall mass transfer (ms^{-1})
x, r	cylindrical coordinates (m)

Greek symbols

φ_1	nanoparticle volume fractions for Al_2O_3 (alumina)
φ_2	nanoparticle volume fractions for Cu (copper)
γ	eigenvalue
η	similarity variable
λ	moving parameter
θ	dimensionless temperature
ϕ	dimensionless nanoparticle concentration
μ	dynamic viscosity of the fluid ($kgm^{-1}s^{-1}$)
ν	kinematic viscosity of the fluid (m^2s^{-1})
ρ	density of the fluid (kgm^{-3})
τ_w	skin friction or wall shear stress ($kgm^{-1}s^{-2}$)
τ	dimensionless time
σ	ratio of effective heat capacity

Subscripts

f	fluid
nf	nanofluid
hnf	hybrid nanofluid
$n1$	solid component for Al_2O_3 (alumina)
$n2$	solid component for Cu (copper)

Superscript

$'$	differentiation with respect to η

References

1. Choi, S.U.S.; Eastman, J.A. Enhancing thermal conductivity of fluids with nanoparticles. In Proceedings of the 1995 ASME International Mechanical Engineering Congress and Exhibition FED 231MD, San Francisco, CA, USA, 12–17 November 1995; pp. 99–105.
2. Khanafer, K.; Vafai, K.; Lightstone, M. Buoyancy-driven heat transfer enhancement in a two-dimensional enclosure utilizing nanofluids. *Int. J. Heat Mass Transf.* **2003**, *46*, 3639–3653. [CrossRef]
3. Oztop, H.F.; Abu-Nada, E. Numerical study of natural convection in partially heated rectangular enclosures filled with nanofluids. *Int. J. Heat Fluid Flow* **2008**, *29*, 1326–1336. [CrossRef]
4. Turcu, R.; Darabont, A.; Nan, A.; Aldea, N.; Macovei, D.; Bica, D.; Vekas, L.; Pana, O.; Soran, M.L.; Koos, A.A.; et al. New polypyrrole-multiwall carbon nanotubes hybrid materials. *J. Optoelectron. Adv. Mater.* **2006**, *8*, 643–647.
5. Jana, S.; Salehi-Khojin, A.; Zhong, W.H. Enhancement of fluid thermal conductivity by the addition of single and hybrid nano-additives. *Thermochim. Acta* **2007**, *462*, 45–55. [CrossRef]

6.   Sarkar, J.; Ghosh, P.; Adil, A. A review on hybrid nanofluids: Recent research, development and applications. *Renew. Sustain. Energy Rev.* **2015**, *43*, 164–177. [CrossRef]

7.   Hemmat Esfe, M.; Alirezaie, A.; Rejvani, M. An applicable study on the thermal conductivity of SWCNT-MgO hybrid nanofluid and price-performance analysis for energy management. *Appl. Therm. Eng.* **2017**, *111*, 1202–1210. [CrossRef]

8.   Devi, S.P.A.; Devi, S.S.U. Numerical investigation of hydromagnetic hybrid Cu-Al$_2$O$_3$/water nanofluid flow over a permeable stretching sheet with suction. *Int. J. Nonlinear Sci. Numer. Simul.* **2016**, *17*, 249–257. [CrossRef]

9.   Devi, S.S.U.; Devi, S.P.A. Numerical investigation of three-dimensional hybrid Cu-Al$_2$O$_3$/water nanofluid flow over a stretching sheet with effecting Lorentz force subject to Newtonian heating. *Can. J. Phys.* **2016**, *94*, 490–496. [CrossRef]

10.   Suresh, S.; Venkitaraj, K.P.; Selvakumar, P.; Chandrasekar, M. Synthesis of Al$_2$O$_3$-Cu/water hybrid nanofluids using two step method and its thermo physical properties. *Colloids Surf. A Physicochem. Eng. Asp.* **2011**, *388*, 41–48. [CrossRef]

11.   Hayat, T.; Nadeem, S. Heat transfer enhancement with Ag-CuO/water hybrid nanofluid. *Results Phys.* **2017**, *7*, 2317–2324. [CrossRef]

12.   Waini, I.; Ishak, A.; Pop, I. Unsteady flow and heat transfer past a stretching/shrinking sheet in a hybrid nanofluid. *Int. J. Heat Mass Transf.* **2019**, *136*, 288–297. [CrossRef]

13.   Waini, I.; Ishak, A.; Pop, I. Flow and heat transfer along a permeable stretching/shrinking curved surface in a hybrid nanofluid. *Phys. Scr.* **2019**, *94*, 105219. [CrossRef]

14.   Waini, I.; Ishak, A.; Pop, I. Hybrid nanofluid flow and heat transfer over a nonlinear permeable stretching/shrinking surface. *Int. J. Numer. Methods Heat Fluid Flow* **2019**, *29*, 3110–3127. [CrossRef]

15.   Waini, I.; Ishak, A.; Pop, I. Hybrid nanofluid flow and heat transfer past a vertical thin needle with prescribed surface heat flux. *Int. J. Numer. Methods Heat Fluid Flow* **2019**, *29*, 4875–4894. [CrossRef]

16.   Waini, I.; Ishak, A.; Pop, I. Transpiration effects on hybrid nanofluid flow and heat transfer over a stretching/shrinking sheet with uniform shear flow. *Alex. Eng. J.* **2020**, *59*, 91–99. [CrossRef]

17.   Waini, I.; Ishak, A.; Pop, I. Hybrid nanofluid flow induced by an exponentially shrinking sheet. *Chin. J. Phys.* **2020**, (in press). [CrossRef]

18.   Waini, I.; Ishak, A.; Pop, I. MHD flow and heat transfer of a hybrid nanofluid past a permeable stretching/shrinking wedge. *Appl. Math. Mech. Engl. Ed.* **2020**, *41*, 507–520. [CrossRef]

19.   Waini, I.; Ishak, A.; Pop, I. Hybrid nano fluid flow and heat transfer over a permeable biaxial stretching/shrinking sheet. *Int. J. Numer. Methods Heat Fluid Flow* **2020**, (in press). [CrossRef]

20.   Waini, I.; Ishak, A.; Groşan, T.; Pop, I. Mixed convection of a hybrid nanofluid flow along a vertical surface embedded in a porous medium. *Int. Commun. Heat Mass Transf.* **2020**, *114*, 104565. [CrossRef]

21.   Lee, L.L. Boundary layer over a thin needle. *Phys. Fluids* **1967**, *10*, 820–822. [CrossRef]

22.   Narain, J.P.; Uberoi, M.S. Forced heat transfer over thin needles. *J. Heat Transf.* **1972**, *94*, 240–242. [CrossRef]

23.   Narain, J.P.; Uberoi, M.S. Laminar free convection from vertical thin needles. *Phys. Fluids* **1972**, *15*, 928–929. [CrossRef]

24.   Narain, J.P.; Uberoi, M.S. Combined forced and free-convection over thin needles. *Int. J. Heat Mass Transf.* **1973**, *16*, 1505–1512. [CrossRef]

25.   Cebeci, T.; Na, T.Y. Laminar free-convection heat transfer from a needle. *Phys. Fluids* **1969**, *12*, 463–465. [CrossRef]

26.   Chen, J.L.S.; Smith, T.N. Forced convection heat transfer from nonisothermal thin needles. *J. Heat Transf.* **1978**, *100*, 358–362. [CrossRef]

27.   Wang, C.Y. Mixed convection on a vertical needle with heated tip. *Phys. Fluids A Fluid Dyn.* **1990**, *2*, 622–625. [CrossRef]

28.   Kafoussias, N.G. Mixed free convection and mass transfer flow along a vertical needle. *Int. J. Energy Res.* **1992**, *16*, 43–49. [CrossRef]

29.   Ahmad, S.; Arifin, N.M.; Nazar, R.; Pop, I. Mixed convection boundary layer flow along vertical thin needles: Assisting and opposing flows. *Int. Commun. Heat Mass Transf.* **2008**, *35*, 157–162. [CrossRef]

30.   Ishak, A.; Nazar, R.; Pop, I. Boundary layer flow over a continuously moving thin needle in a parallel free stream. *Chin. Phys. Lett.* **2007**, *24*, 2895–2897. [CrossRef]

31. Waini, I.; Ishak, A.; Pop, I. On the stability of the flow and heat transfer over a moving thin needle with prescribed surface heat flux. *Chin. J. Phys.* **2019**, *60*, 651–658. [CrossRef]

32. Grosan, T.; Pop, I. Forced convection boundary layer flow past nonisothermal thin needles in nanofluids. *J. Heat Transf.* **2011**, *133*, 054503. [CrossRef]

33. Soid, S.K.; Ishak, A.; Pop, I. Boundary layer flow past a continuously moving thin needle in a nanofluid. *Appl. Therm. Eng.* **2017**, *114*, 58–64. [CrossRef]

34. Salleh, S.N.A.; Bachok, N.; Arifin, N.M.; Ali, F.M.; Pop, I. Magnetohydrodynamics flow past a moving vertical thin needle in a nanofluid with stability analysis. *Energies* **2018**, *11*, 3297. [CrossRef]

35. Tiwari, R.K.; Das, M.K. Heat transfer augmentation in a two-sided lid-driven differentially heated square cavity utilizing nanofluids. *Int. J. Heat Mass Transf.* **2007**, *50*, 2002–2018. [CrossRef]

36. Buongiorno, J. Convective transport in nanofluids. *J. Heat Transf.* **2006**, *128*, 240–250. [CrossRef]

37. Kuznetsov, A.V.; Nield, D.A. Natural convective boundary-layer flow of a nano fluid past a vertical plate: A revised model. *Int. J. Therm. Sci.* **2014**, *77*, 126–129. [CrossRef]

38. Merkin, J.H. On dual solutions occurring in mixed convection in a porous medium. *J. Eng. Math.* **1986**, *20*, 171–179. [CrossRef]

39. Weidman, P.D.; Kubitschek, D.G.; Davis, A.M.J. The effect of transpiration on self-similar boundary layer flow over moving surfaces. *Int. J. Eng. Sci.* **2006**, *44*, 730–737. [CrossRef]

40. Harris, S.D.; Ingham, D.B.; Pop, I. Mixed convection boundary-layer flow near the stagnation point on a vertical surface in a porous medium: Brinkman model with slip. *Transp. Porous Media* **2009**, *77*, 267–285. [CrossRef]

41. Shampine, L.F.; Gladwell, I.; Thompson, S. *Solving ODEs with MATLAB*; Cambridge University Press: Cambridge, UK, 2003; ISBN 9780521824040.

42. Awaludin, I.S.; Ishak, A.; Pop, I. On the stability of MHD boundary layer flow over a stretching/shrinking wedge. *Sci. Rep.* **2018**, *8*, 13622. [CrossRef]

43. Soid, S.K.; Ishak, A.; Pop, I. MHD stagnation-point flow over a stretching/shrinking sheet in a micropolar fluid with a slip boundary. *Sains Malays.* **2018**, *47*, 2907–2916. [CrossRef]

44. Kamal, F.; Zaimi, K.; Ishak, A.; Pop, I. Stability analysis of MHD stagnation-point flow towards a permeable stretching/shrinking sheet in a nanofluid with chemical reactions effect. *Sains Malays.* **2019**, *48*, 243–250. [CrossRef]

45. Jusoh, R.; Nazar, R.; Pop, I. Magnetohydrodynamic boundary layer flow and heat transfer of nanofluids past a bidirectional exponential permeable stretching/shrinking sheet with viscous dissipation effect. *J. Heat Transf.* **2019**, *141*, 012406. [CrossRef]

46. Khashi'ie, N.S.; Arifin, N.M.; Nazar, R.; Hafidzuddin, E.H.; Wahi, N.; Pop, I. A stability analysis for magnetohydrodynamics stagnation point flow with zero nanoparticles flux condition and anisotropic slip. *Energies* **2019**, *12*, 1268. [CrossRef]